High-Speed Multiplexed DNA-PAINT Imaging of Nuclear Organization Using an Expanded Sequence Repertoire

Abhinav Banerjee[1, #], Micky Anand[1, #], Mansi Srivastava[1], Vedanth Shree Vidwath[1], Mahipal Ganji[1, *]

[1]Department of Biochemistry, Indian Institute of Science, Malleswaram, Bangalore-560012, India.

[#] Equal contribution

*Correspondence: ganji@iisc.ac.in, Phone: +91 80 2293 2309

Abstract

DNA-Points Accumulation for Imaging in Nanoscale Topography (DNA-PAINT) enables multiplexed super-resolution imaging of biological samples. We expand the repertoire of speed-optimized DNA sequences for DNA-PAINT imaging to drive visualization of ten targets in a sequential manner with molecular resolution. We demonstrate this by visualizing diverse nuclear targets and characterizing their relative spatial distribution. We outline major reorganization in the chromatin landscape upon transcription inhibition. The ability to image as many as ten targets using this strategy at accelerated speed will drive its further adoption for diverse cellular imaging applications.

Main

Recent years have witnessed tremendous development in a variety of super-resolution imaging techniques, which enable us to gain greater insights into the spatial distribution of biomolecules at nanometer resolution in intact cells[1-4]. DNA-PAINT, a variant of Single-Molecule Localization Microscopy, achieves diffraction unlimited resolution through stochastic, transient hybridization of short complementary single-stranded DNAs.[2-5] Additionally, DNA-PAINT enables multiplexed imaging by encoding the target identity into DNA docking strand. However, the acquisition times are enormous, requiring up to several hours for each imaging round,[6] because of the rather slow binding kinetics of initial DNA sequences[6,7]. Recent studies have improved imaging speed by cleverly designing imager strands with non-complementary nucleotides arranged in repetitive blocks forming concatenated sequences.[4,8]

Currently, only six speed-optimized sequences are available, limiting multiplexing to six targets. Although recent studies using secondary[9] or adapter DNA probes[10] allow near-unlimited multiplexing, they require complex strand hybridization and dissociation schemes.[11] Thus, expanding the sequence space to enable faster imaging with greater multiplexing-ability remains a key challenge.

To address this, we systematically searched for all possible imager-docking strand pairs that support faster imaging. Two design rules that were followed in this search are that (1) the imager strand must not comprise nucleotides that are complementary, and (2) they must form units that can be concatenated to form overlapped docking strands[12] (Supplementary Figure 1a, b). This yielded two di-, four tri-, and six tetra-nucleotide blocks (Figure 1a, Supplementary Figure 1c). We reserved cytosines (C) containing blocks for docking strands, and guanines (G) containing blocks for imagers. These sequences preclude secondary structures, promoting rapid and efficient binding. Concatenation of such blocks further improve binding rates by increasing the number potential binding sites. Using this strategy, we propose as many as 12 sequences of which six sequences were reported earlier[12] (Figure 1b). Increasing the block length to five nucleotides compromises orthogonality and was hence excluded from further consideration (Supplementary figure 1d).

We tested the multiplexing capability of all speed-optimized sequences utilizing unique DNA nanostructures carrying docking strands for each of the imager sequences. For visual identification and testing the resolution, we designed origami nanostructures carrying docking strands in a 4×3 grid pattern where each strand is separated from its neighbor by 20 nm. We immobilized these in a single microfluidic channel and imaged them in 12 rounds using Exchange-PAINT modality[5] (Figure 1c). As expected, all 12 species of origami nanostructures were clearly visible in the merged data (Figure 1d). While majority of the imagers showed clear specific binding on their target docking strands, two sets of imagers (R1 and R9, R2 and R10) displayed unexpected non-specific binding (Figure 1e), emphasizing the tolerance for certain DNA mismatches to form detectable duplexes. Because of this cross-binding, only one imager from each of these pairs can be used for multiplexed imaging. Together, Exchange-PAINT imaging of “12-color” data shows that we can achieve multiplexing capabilities of as many as ten targets at high-speed and high-resolution (Figure 1d, 1e and Supplementary Figure 2).

We next performed kinetic analysis of all twelve imager-docking strands by utilizing DNA nanostructures with patterns carrying a unique docking strand in the center (Supplementary Figure 3a). We performed two-color DNA-PAINT imaging to obtain the pattern of the nanostructure and kinetics of the docking strand (Supplementary Figure 3b). Our analysis shows that these imagers display a range of binding times from few hundred milli-seconds to over a second (Figure 1f and Supplementary Figure 3c). This versatile imager pool with varying binding times enables us to utilize imager strands based on the required properties for a given imaging application. For instance, imagers with wide range of kinetics can enhance the multiplexing capabilities of DNA-PAINT via kinetic barcoding[13,14].

We tested their applicability for studying nuclear targets by imaging Lamin B1 in cellular settings and found that all the imagers showed the expected signals, except R3, which additionally marked the nucleolar structure non-specifically (Supplementary Figure 4 and 5). These data reveal that nine-color imaging of nuclear targets with an Exchange-PAINT based approach is readily possible at enhanced speeds.

We then strategized to exploit these sequences to delineate the spatial distribution of various nuclear features. We targeted nine different nuclear marks encompassing features known to delineate euchromatin (RNA pol II Serine 2 Phosphorylation (S2P), RNA pol II Serine 5 Phosphorylation (S5P), splicing factor SC35, H3K4me3 and H3K37ac); heterochromatin (H3K27me3, H3K9me3, Lamin B1); and CTCF, a transcription factor involved in dictating genome architecture. For achieving multiplexed imaging with the same species primary antibodies, we preincubated them with secondary nanobodies, each conjugated to a distinct DNA docking strand (Figure 2a).[9,10] This strategy avoids cross-reactivity and enabled us to visualize multiple nuclear targets using DNA-PAINT. The differential distribution of all targets relative to each other showcases the complexity of nuclear organization in a single cell captured through multiplexed imaging (Figure 2b, Supplementary Figure 6 (top)).

To further benchmark our approach, we imaged transcriptionally impaired cells treated with Actinomycin D, which profoundly altered spatial nuclear organization (Figure 2c, Supplementary Figure 6 (bottom) and 7). To further benchmark our approach, we imaged transcriptionally impaired cells treated with Actinomycin D[15], which profoundly altered spatial nuclear organization (Figure 2c, Supplementary Figure 6 (bottom) and 7). Surprisingly, Lamin

B1 delocalized from the nuclear periphery to the interiors of the nucleus. This is accompanied by loss of distinct nuclear speckle bodies demarcated by SC35 enrichment, as observed in mock cells. These results exemplify the robustness of multiplexed imaging in capturing these redistributions in a single cell.

To quantitatively interpret our data, we employed a coarse-grained correlation analysis between target pairs (see Methods). We observe expected associations among these targets in the DMSO-treated (mock) cells.[16] For instance, RNApolII-S2P and RNApolII-S5P show positive correlation with the splicing factor SC35, indicating their physical proximity. Similarly, heterochromatin marks correlate with nuclear lamin (Figure 3a–below diagonal). We also observed expected mutual exclusion of euchromatin and heterochromatin marks. Upon transcription inhibition, we observed a complete reorganization of all the factors with increased positive correlation amongst them (Figure 3a–above diagonal). Interestingly, SC35 displayed a negative correlation with all nuclear components (Figure 3a).

Leveraging on our high-resolution data, we next performed spatial correlation viewpoint analysis between each pair of targets. This analyses once again embodies the correlation amongst heterochromatin and euchromatin regions. Heterochromatin marks show a clear mutual interaction. Additionally, SC35 shows a distinct preference to euchromatin, emphasized by the larger fractions showing high-positive correlation (<0.7) and low fractions showing high-negative correlation (<-0.7) with euchromatin marks. Under ActD treatment, we observe a marked loss in fractions showing high positive correlation of SC35 with euchromatin marks and a corresponding gain in negative correlations (Figure 3b, Supplementary Figure 8 and 9). This indicates a likely loss of contacts between SC35 and chromatin regions. In contrast, a gain in all fractions showing high positive correlation between all other interactions indicate chromatin collapse, corroborating earlier reported observations[17].In contrast, a gain in all fractions showing high positive correlation between all other interactions indicate chromatin collapse, corroborating earlier reported observations[17].

Given the high density of nuclear content, it is apparent to observe palpable correlations between nuclear features due to their proximity. However, spatial correlation maps enable us to discern regions where interactions are significantly higher and correlate better with the

target of interest. To investigate this further, we chose two viewpoints: Lamin B1 to represent heterochromatic organization and SC35 to represent euchromatic organization. In untreated cells, both heterochromatic marks (H3K9me3 and H3K27me3) and actively transcribing RNA pol II (RNApolII-S2P and -S5P) show high positive enrichment near their respective viewpoints of lamin and nuclear speckle, respectively (Figure 3c top, Full nucleus view). Zoomed-in regions further emphasize this observation where all other targets show diminishing enrichments near the lamin, with actively transcribing RNA pol II marks (RNApolII-S2P and -S5P) showing the least enrichment of high-correlation at 6.16% and 5.40% respectively. From the SC35 viewpoint, similar diminishing trends are observed, with H3K9me3 and Lamin B1 showing the least enrichment of 8.14%. and 3.92% respectively.

Upon transcription inhibition, highly correlating regions of both heterochromatic marks show discernable delocalization from the nuclear periphery, indicating a loss of peripheral enrichment of these marks alongside Lamin B1 internalization. Nuclear speckles, though lower in number, no longer show distinct enrichment of actively transcribing RNApolII (Figure 3c bottom, Full nucleus view). Zoom-in views reveal a distinct pattern of higher correlating regions–most targets are enriched with lamin B1 in small pockets distributed within the nucleus, rather than at the nuclear periphery. Conversely, we clearly observe a loss in correlation of almost all targets near the nuclear speckles further highlighting the changes in spatial organization of chromatin due to transcription inhibition and chromatin collapse.

The expansion of speed-optimized imager-docking strand sequences will unlock the full potential of DNA-PAINT imaging's multiplexing capabilities. Additionally, the adapter-strand-based "unlimited" multiplexing can be done in batches of ten instead of six targets per labeling round which would drastically reduce the time required for multiplexing. The increased repertoire of speed-optimized imager-docking strand sequences will also facilitate multi-color sub-nanometer resolution imaging with RESI which requires multiple rounds of imaging for each target identification.[18] Simultaneous imaging of histone modifications, transcriptional machinery, and nuclear bodies at high resolution, signify the application of new sequences in the field of spatial proteomics and interactome building, in addition to other allied fields including biomedical sciences.

Figure Captions:

Figure 1: Full repertoire of imager strands for high-speed DNA-PAINT and their binding kinetics. (a) All possible building blocks for constructing imager strands. (b) The sequences of all 12 imager strands. (c) Scheme for 12-color multiplexed imaging using Exchange-PAINT. (d) Merged 12-color DNA-PAINT data of DNA origami nanostructures. (e) Chart showing orthogonality and cross-binding of imagers. Red squares depict unexpected cross-binding. Green squares depict specific binding. (f) Scatter plot showing average of individual binding times per binding site of each docking strand. In (b) and (f), 'existing' refers to imagers reported earlier.[12] (Scale: (d) 500nm)

Figure 2: Nine–plex imaging of the nucleus. (a) Experimental scheme. (i) Preincubation of primary antibodies with DNA conjugated secondary nanobodies. (ii) Cells grown in glass bottom 8-well dishes. (iii) Nine nuclear marks imaged in sequential imaging rounds; Nine-plex images of single nuclei showing detailed organization of targets in (b) mock (left) and (c) ActD (right) treated cells. (Scale: (b) 5 µm)

Figure 3: Transcription inhibition perturbs nuclear organization at multiple scales. (a) Global Pearson correlation heatmap showing spatial relationships among nine nuclear marks in control (Mock, cyan) and transcription inhibited cells (ActD, magenta) cells (b) Fraction of localizations exhibiting strong Spearman correlation ($\rho > 0.7$ or $\rho < -0.7$) with other targets. (c) Viewpoint analyses of spatial correlations. Full cells: Localizations with high positive correlation ($\rho > 0.7$) of H3K27me3 (Blue) and H3K9me3 (Violet) with Lamin B1 (Black) in the Lamin viewpoint sections, and S2P (Red) and S5P (Golden-Yellow) with SC35 (Black) in the SC35 viewpoint, respectively, in mock and ActD treated cells. Zoom Ins: First row – all localization for the respective target (in color) and localizations for Lamin B1 or SC35 (in black), respectively. Second row – KDE plots of the spatial correlations for all localization of the target with the reference (Lamin B1 and SC35 respectively) in first row. Shaded portion shows high positive correlations ($\rho > 0.7$). Percentage of points with high spatial correlation is outlined. Third row – spatial distribution of localizations with high positive correlation ($\rho > 0.7$) with the reference, respectively. Looped models represent likely chromatin distribution.

References

1 Hell, S. W. & Wichmann, J. Breaking the diffraction resolution limit by stimulated emission: stimulated-emission-depletion fluorescence microscopy. *Opt Lett* **19**, 780-782 (1994).

2 Betzig, E. *et al.* Imaging intracellular fluorescent proteins at nanometer resolution. *Science* **313**, 1642-1645 (2006). https://doi.org/10.1126/science.1127344

3 Rust, M. J., Bates, M. & Zhuang, X. Sub-diffraction-limit imaging by stochastic optical reconstruction microscopy (STORM). *Nat Methods* **3**, 793-795 (2006). https://doi.org/10.1038/nmeth929

4 Jungmann, R. *et al.* Single-molecule kinetics and super-resolution microscopy by fluorescence imaging of transient binding on DNA origami. *Nano Lett* **10**, 4756-4761 (2010). https://doi.org/10.1021/nl103427w

5 Jungmann, R. *et al.* Multiplexed 3D cellular super-resolution imaging with DNA-PAINT and Exchange-PAINT. *Nat Methods* **11**, 313-318 (2014). https://doi.org/10.1038/nmeth.2835

6 Schlichthaerle, T., Ganji, M., Auer, A., Kimbu Wade, O. & Jungmann, R. Bacterially Derived Antibody Binders as Small Adapters for DNA-PAINT Microscopy. *Chembiochem* **20**, 1032-1038 (2019). https://doi.org/10.1002/cbic.201800743

7 Fischer, L. S. *et al.* Quantitative single-protein imaging reveals molecular complex formation of integrin, talin, and kindlin during cell adhesion. *Nature Communications* **12**, 919 (2021). https://doi.org/10.1038/s41467-021-21142-2

8 Schnitzbauer, J., Strauss, M. T., Schlichthaerle, T., Schueder, F. & Jungmann, R. Super-resolution microscopy with DNA-PAINT. *Nature protocols* **12**, 1198-1228 (2017).

9 Unterauer, E. M. *et al.* Spatial proteomics in neurons at single-protein resolution. *Cell* **187**, 1785-1800.e1716 (2024). https://doi.org/https://doi.org/10.1016/j.cell.2024.02.045

10 Schueder, F. *et al.* Unraveling cellular complexity with transient adapters in highly multiplexed super-resolution imaging. *Cell* **187**, 1769-1784.e1718 (2024). https://doi.org/https://doi.org/10.1016/j.cell.2024.02.033

11 Lycas, M. D. & Manley, S. DNA-PAINT adaptors make for efficient multiplexing. *Cell Reports Methods* **4** (2024). https://doi.org/10.1016/j.crmeth.2024.100801

12 Strauss, S. & Jungmann, R. Up to 100-fold speed-up and multiplexing in optimized DNA-PAINT. *Nat Methods* **17**, 789-791 (2020). https://doi.org/10.1038/s41592-020-0869-x

13 Banerjee, A., Anand, M., Kalita, S. & Ganji, M. Single-molecule analysis of DNA base-stacking energetics using patterned DNA nanostructures. *Nature Nanotechnology* **18**, 1474-1482 (2023).

14 Wade, O. K. *et al.* 124-Color super-resolution imaging by engineering DNA-PAINT blinking kinetics. *Nano letters* **19**, 2641-2646 (2019).

15 Sobell, H. M. Actinomycin and DNA transcription. *Proceedings of the National Academy of Sciences* **82**, 5328-5331 (1985).

16 Hattori, N., Niwa, T., Kimura, K., Helin, K. & Ushijima, T. Visualization of multivalent histone modification in a single cell reveals highly concerted epigenetic changes on differentiation of embryonic stem cells. *Nucleic Acids Research* **41**, 7231-7239 (2013). https://doi.org/10.1093/nar/gkt528

17 Neguembor, M. V. *et al.* Transcription-mediated supercoiling regulates genome folding and loop formation. *Molecular cell* **81**, 3065-3081. e3012 (2021).

18 Reinhardt, S. C. M. *et al.* Ångström-resolution fluorescence microscopy. *Nature* **617**, 711-716 (2023). https://doi.org/10.1038/s41586-023-05925-9

Acknowledgements

We acknowledge Vinay Bhardwaj for helping with purifying anti-rabbit IgG secondary nanobody. A.B. and M.A. acknowledge the support from the Prime Minister's Research Fellowship (PMRF), Ministry of Education, Government of India. We greatly acknowledge Sarit Agasti for allowing us to use their laboratory facilities and S. Kalita for help with HPLC purification of DNA imager strands.

Funding Sources

We also acknowledge Department of Science and Technology, Ministry of Science and Technology, India DST-FIST Program funded Central Facility, Department of Biochemistry, IISc. This work has been supported in part by a DBT/Wellcome India Alliance intermediate fellowship (IA/I/21/2/505928) and the Department of Biotechnology (BT/PR40186/BTIS/137/3/2020). We greatly acknowledge the support from Max-Planck Institute of Immunology and Epigenetics Freiburg, Germany in terms of partner group to Mahipal Ganji lab.

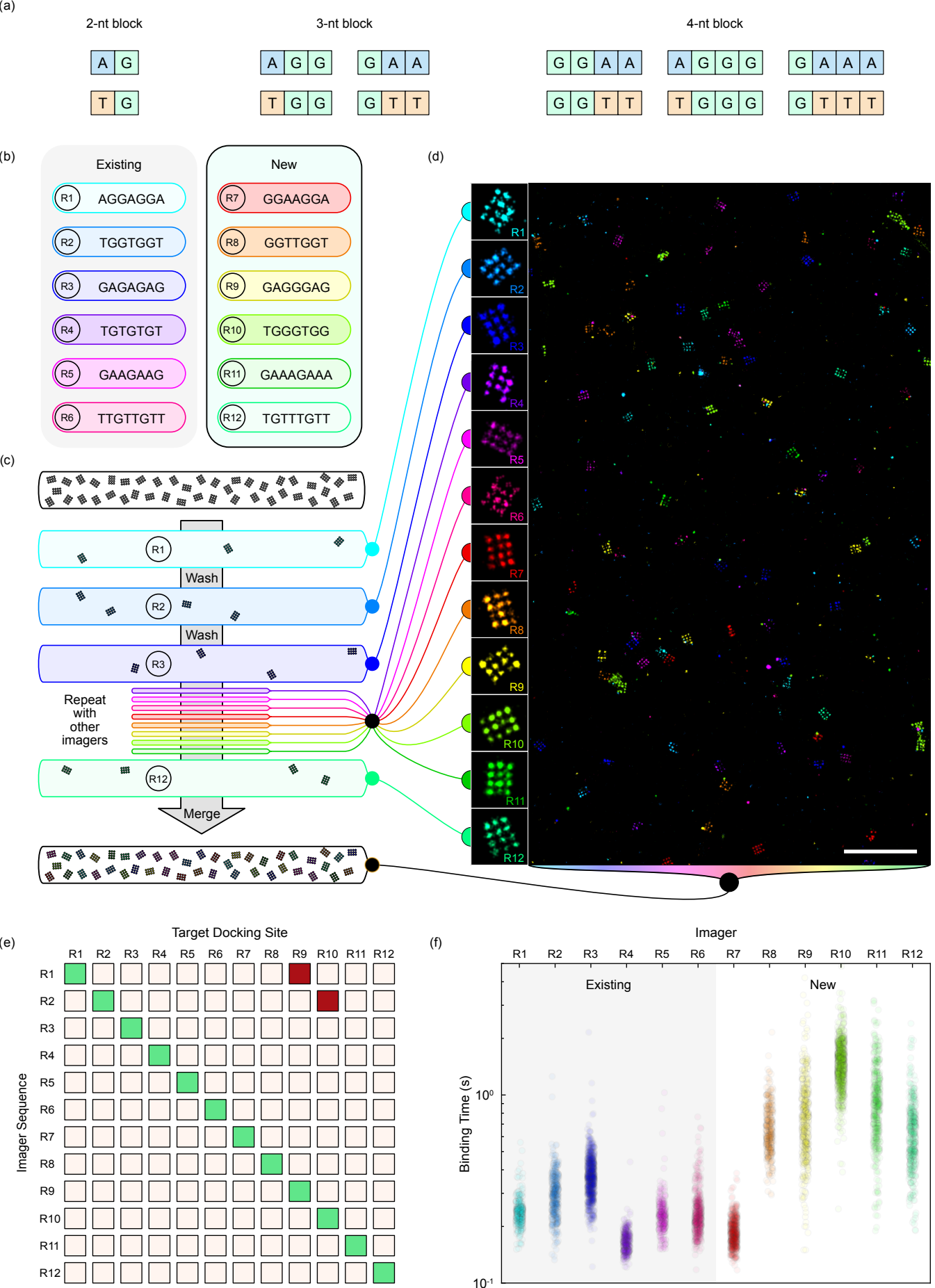
(a)
2-nt block
A G
T G
3-nt block
A G G
T G G
G A A
G T T
4-nt block
G G A A
G G T T
A G G G
T G G G
G A A A
G T T T
(b)
Existing
R1 AGGAGGA
R2 TGGTGGT
R3 GAGAGAG
R4 TGTGTGT
R5 GAAGAAG
R6 TTGTTGTT
New
R7 GGAAGGA
R8 GGTTGGT
R9 GAGGGAG
R10 TGGGTGG
R11 GAAAGAAA
R12 TGTTTGTT
(c)
R1
Wash
R2
Wash
R3
Repeat with other imagers
R12
Merge
(d)
R1
R2
R3
R4
R5
R6
R7
R8
R9
R10
R11
R12
(e)
Target Docking Site
R1 R2 R3 R4 R5 R6 R7 R8 R9 R10 R11 R12
Imager Sequence
R1
R2
R3
R4
R5
R6
R7
R8
R9
R10
R11
R12
(f)
Imager
R1 R2 R3 R4 R5 R6 R7 R8 R9 R10 R11 R12
Existing
New
Binding Time (s)
10^0
10^{-1}

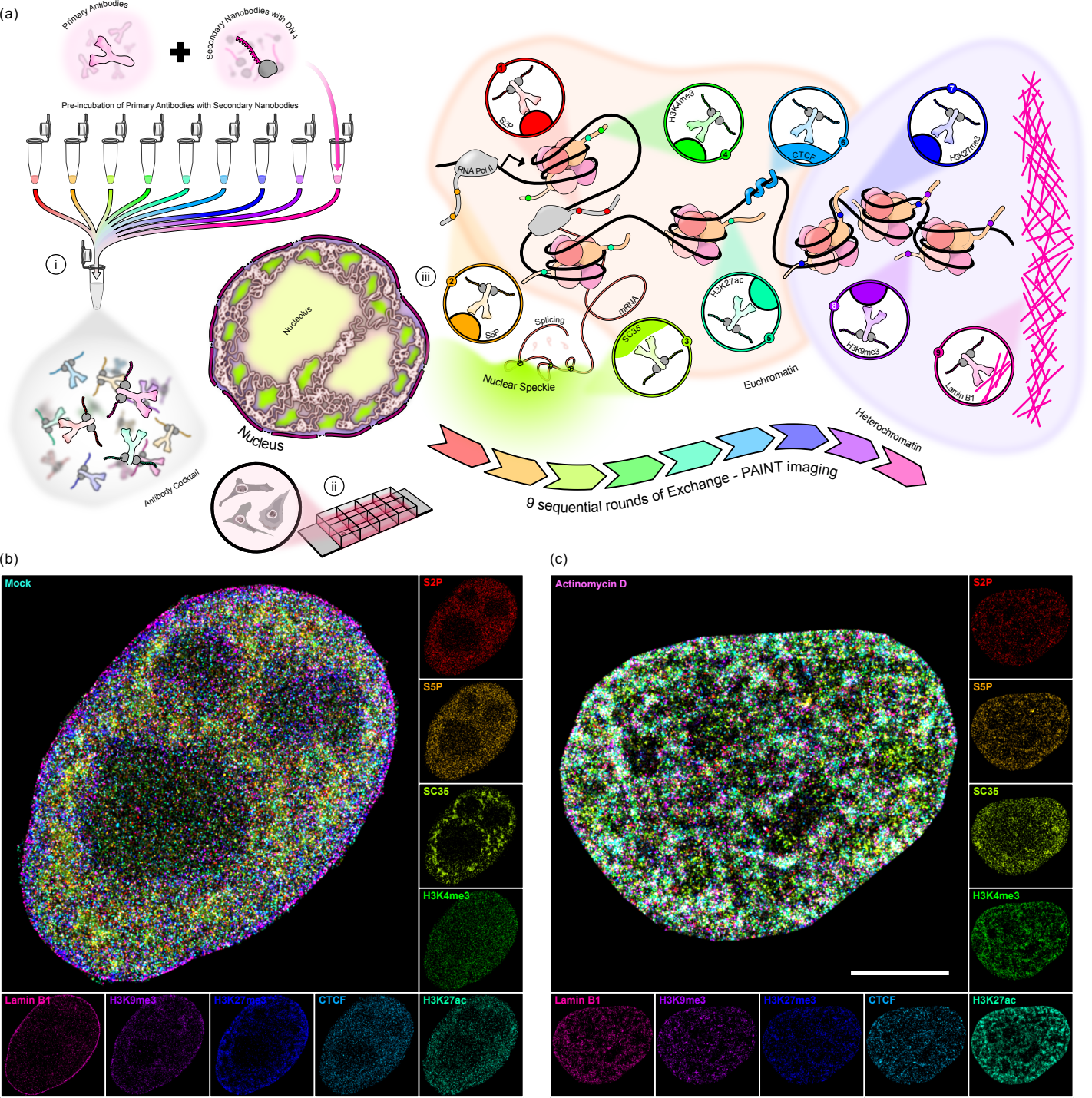
(a)
Primary Antibodies
Secondary Nanobodies with DNA
Pre-incubation of Primary Antibodies with Secondary Nanobodies
i
ii
iii
Antibody Cocktail
Nucleus
Nucleolus
RNA Pol II
S2P
S5P
SC35
H3K4me3
CTCF
H3K27ac
H3K27me3
H3K9me3
Lamin B1
mRNA
Splicing
Nuclear Speckle
Euchromatin
Heterochromatin
9 sequential rounds of Exchange - PAINT imaging
(b)
Mock
S2P
S5P
SC35
H3K4me3
Lamin B1
H3K9me3
H3K27me3
CTCF
H3K27ac
(c)
Actinomycin D
S2P
S5P
SC35
H3K4me3
Lamin B1
H3K9me3
H3K27me3
CTCF
H3K27ac

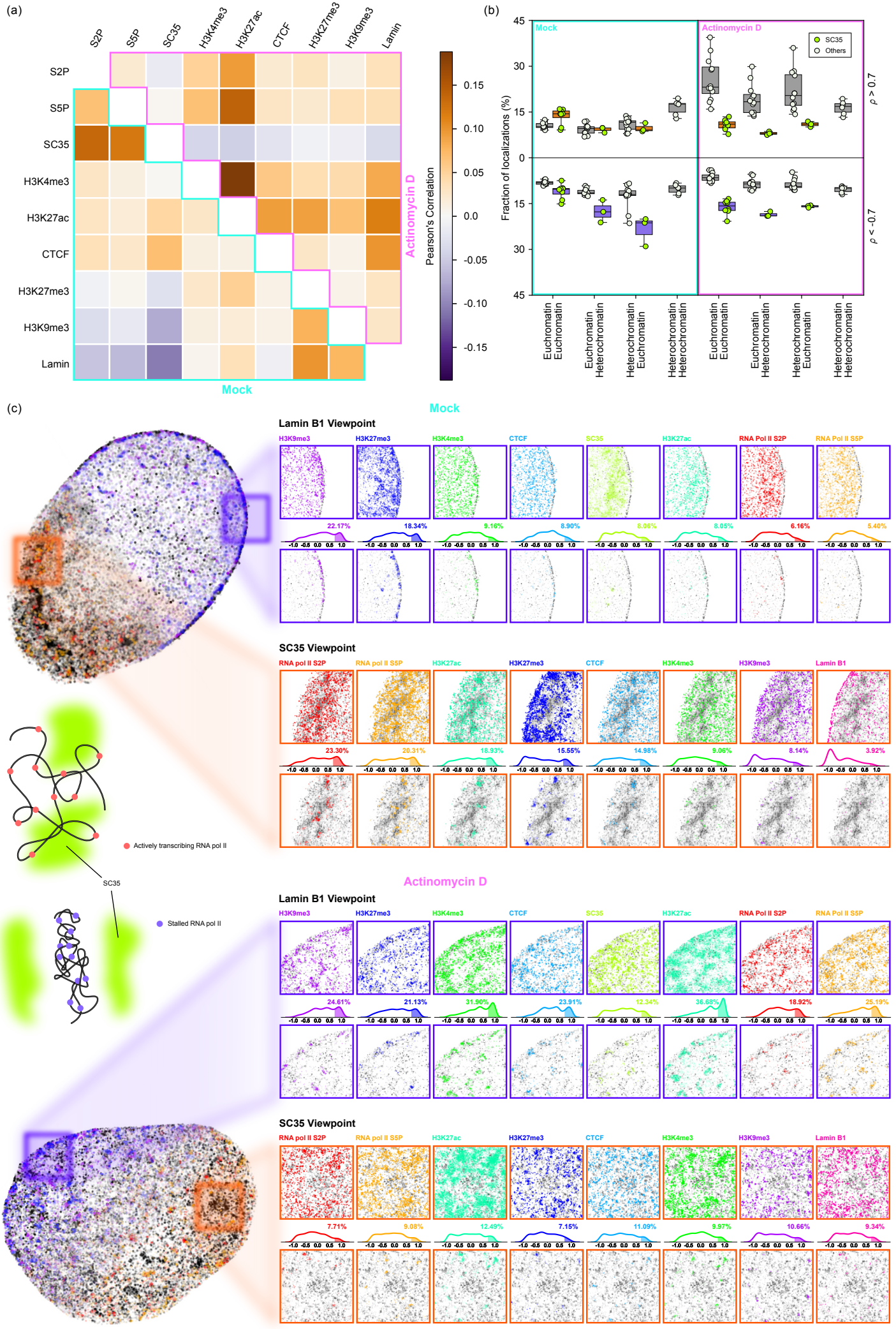
(a)
S2P
S5P
SC35
H3K4me3
H3K27ac
CTCF
H3K27me3
H3K9me3
Lamin
Mock
Actinomycin D
Pearson's Correlation
0.15
0.10
0.05
0.0
-0.05
-0.10
-0.15
(b)
Mock
Actinomycin D
SC35
Others
Fraction of localizations (%)
ρ > 0.7
ρ < -0.7
Euchromatin Euchromatin
Euchromatin Heterochromatin
Heterochromatin Euchromatin
Heterochromatin Heterochromatin
(c)
Mock
Lamin B1 Viewpoint
H3K9me3
H3K27me3
H3K4me3
CTCF
SC35
H3K27ac
RNA Pol II S2P
RNA Pol II S5P
22.17%
18.34%
9.16%
8.90%
8.06%
8.05%
6.16%
5.40%
SC35 Viewpoint
RNA pol II S2P
RNA pol II S5P
H3K27ac
H3K27me3
CTCF
H3K4me3
H3K9me3
Lamin B1
23.30%
20.31%
18.93%
15.55%
14.98%
9.06%
8.14%
3.92%
Actively transcribing RNA pol II
SC35
Stalled RNA pol II
Actinomycin D
Lamin B1 Viewpoint
24.61%
21.13%
31.90%
23.91%
12.34%
36.68%
18.92%
25.19%
SC35 Viewpoint
7.71%
9.08%
12.49%
7.15%
11.09%
9.97%
10.66%
9.34%